Feature Correspondence with Even Distribution

Xiao Tan*, Changming Sun†, Xavier Sirault‡, Robert Furbank‡ and Tuan D. Pham§

*School of Engineering and Information Technology
UNSW Canberra, ACT 2610, Australia
Email: xiao.tan@csiro.au

†CSIRO Mathematics, Informatics and Statistics
Locked Bag 17, North Ryde, NSW 1670, Australia
Email: changming.sun@csiro.au

‡CSIRO Plant Industry
Clunies Ross Street, Canberra, ACT 2601, Australia
Email: {xavier.sirault,robert.furbank}@csiro.au

§Aizu Research Cluster for Medical Engineering and Informatics
Research Center for Advanced Information Science and Technology
The University of Aizu, Aizu-Wakamatsu, Fukushima 965-8580, Japan
Email: tdpham@u-aizu.ac.jp

***Abstract*—This paper presents a new method for finding feature correspondences between a pair of stereo images, which can be used to perform 3D reconstruction and object recognition. This paper uses epiploar geometry to determine the location of potential matching points which allow the finding of the correspondences faster and more accurately. An adaptive smoothness algorithm is also proposed to filter out false matches based on the disparity jump in neighboring correspondences. More correspondences are then identified in such a way that they are evenly distributed in the images. Experimental results show that the proposed method effectively improve the percentage of correct matches, total number of correct matches, and even distribution of the correspondences.**

I. Introduction

Finding feature correspondences in a stereo pair has been widely used in various computer vision studies such as fundamental matrix calculation [1], [2], 3D reconstruction [3], [4], camera calibration [5], and object recognition [6], [7]. Two main steps are involved in most existing methods to find the correspondences. In the first step, keypoints are detected and a specific descriptor is calculated for each keypoint within a neighboring region. By comparing the similarity of the descriptors of the candidates and using some constraints the correspondences can be found among the candidates which are detected in the first step.

Many advanced keypoints detectors are proposed, such as the scale invariant feature transform (SIFT) [8], the gradient location and orientation histogram (GLOH) [9], and the speeded up robust features (SURF) [10]. A simple method for finding the correct correspondences is proposed in [8], where the ratio between the best match and the second best match of each keypoint is used to decide whether a matching pair is correct or not. This method uses no extra constraints and is easy to implement; but its disadvantage is that it is sensitive to the selection of the predefined threshold. That is to say if the threshold is high, many correct correspondences will be filtered out; if the threshold is low, many false correspondences will remain in the result. Some studies have been carried out to solve this problem. In [11], the pairwise constraints are used to build an adjacent matrix and the correspondences are found by finding the principal eigenvector. In [12], the false correspondences are rejected according to a geometric constraint. A triangle constraint is used in [13] to find more correspondences. A global solution to sparse correspondence problems is proposed in [14], where the problem of finding correspondences is formulated as an integer optimization problem and then solved by concave programming on a convex set. All the methods described above focus on improving the percentage of correct matches or finding more matching points; but none of them considers the distribution of the correspondences. The accuracy of epipolar geometry can be improved by having evenly distributed matching points in stereo pairs [15], [2], [16]. Thus, a good set of correspondences should have three characteristics: (1) They are matched properly; (2) There are enough matching pairs; and (3) The pairs distributed evenly over the stereo pair images.

This paper presents a novel method to solve the sparse correspondence problem. In our method, the epiploar constraint is used to reduce the search space and improve the percentage of correct matches, and the false correspondences are rejected using the smoothness constraint in the disparity space. Finally more correspondences are found using the distribution of correspondences.

The paper is organized as follow: we introduce our approach in Section II and Section III. The experimental results are

given in Section IV. We conclude our work in Section V.

II. Reliable Feature Correspondences

In this step we do not attempt to find all the correct correspondences in the image pair. We only extract some reliable matching pairs and generate the 3D information about the scene, from which more correspondences can be found in the next step. The reliable matches are found according to the epipolar constraint, the uniqueness constraint, and the 3D smoothness constraint. Let p_i be a keypoint in one image, and q_j be a keypoint in the other image. In our paper we use the same notation for a keypoint and its homogenous coordinate.

A. Uniqueness and Epipolar Constraints

For each keypoint in one image, we find its best matching point from all keypoints in the other image by applying the "winner-take-all" strategy based on the similarity score which is measured by the Euclidean distance between two descriptors. The best matching pair is the one having the smallest distance between two features. The keypoints in one image and their best matching points in the other image form the set of candidate matches. The candidate matches obtained as described above are not symmetric. Different keypoints in one image may have the same best matching point in the other image. If we reverse the role of the two images, the candidate matches may not be the same. In order to eliminate this ambiguity, we employ the uniqueness constraint: if serval keypoints in one image have the same best matching point in the other image, only the point which has the largest similarity score is considered as the candidate match.

Epipolar geometry provides the relation between two images of a single scene, which is described by the fundamental matrix [17], [1], [2]. Consider a candidate match pair (p, q). The epipolar constraint requires:

$$p^T F q = 0 \tag{1}$$

where F is the fundamental matrix which can be calculated using the normalized 8-points algorithm [1]. The matches used in [1] are obtained from the method described in [8]. Although these matches may contain some false matches, we can still obtain an approximate estimation to the fundamental matrix by using robust methods such as LMedS [2] and RANSAC [18].

Let $Fq_j = (l_1, l_2, l_3)^T$, $F^T q_i = (l'_1, l'_2, l'_3)^T$. After calculating the fundamental matrix, we check each pair of candidate match, (p_i, q_j), whether the requirement of its symmetric epipolar constraint is satisfied:

$$w \left| p_i^T F q_j \right| \leq \varepsilon \tag{2}$$

where

$$w = \left(\frac{1}{l_1^2 + l_2^2} + \frac{1}{{l'_1}^2 + {l'_2}^2} \right)^{\frac{1}{2}} \tag{3}$$

Instead of using Eq. (1), we use Eq. (2) for two reasons. First, the obtained fundamental matrix may not be the perfect one. Second, the location error of a keypoint is inevitable even though the match is correct. The parameter ε, the permitted maximum deviation of (p, q) from the epipolar constraint in the pixel domain, is set to 10. It works very well for all the image sets. If a candidate match does not meet the requirement in Eq. (2), it will be eliminated from the set of candidate matches.

B. Adaptive Disparity Smoothness Filter

Consider a candidate match, (p_i, q_j), where i and j are the indices of keypoints in two images. According to the smoothness constraint of the disparity field, if the match (p_i, q_j) is a correct match, the disparity between p_i and q_i should be similar to the disparities of its neighboring matches. On the other hand, if its disparity is different from those of its neighboring matches, it is most likely a false match.

We now introduce our adaptive disparity smoothness filter (ADSF). Here, we call one image the source image where the smoothness filter is applied to, and the other image the reference image. Let $S : P \mapsto Q$ be a set of candidate matches, where P is the set of keypoints in the source image, and Q is the set of keypoints in the reference image. Note that, P is not the set of all keypoints in the source image; it only contains the keypoints in the source image which are matched in S. Q is similarly defined by the matched keypoints in the reference image. For a keypoint p $(p \in P)$, its neighboring keypoints, $N(p)$, are defined by the set of 10 nearest neighboring keypoints of p in P. The disparity of p is denoted by $d(p)$. As the spatial distance of two keypoints increases, the similarity of their disparities decreases [19], [20]. For a keypoint p_r in $N(p)$, its weight respect to p is calculated by:

$$w_r = \frac{\exp\left(-\frac{\|p,p_r\|}{\alpha}\right)}{\sum\limits_{p_i \in N(p)} \exp\left(-\frac{\|p,p_i\|}{\alpha}\right)} \tag{4}$$

where $\|p, p_i\|$ is the Euclidean distance between p and p_i, α is the normalization parameter.

The keypoints in $N(p)$ are sorted into ascending order by their disparities, that is

$$\forall p_i, p_j \in N(p) \quad i < j \Rightarrow d(p_i) \leq d(p_j) \tag{5}$$

We define the weighted median disparity (wMd) for a keypoint p by

$$d_{wm}(p) = d(p_{wm}) \tag{6}$$

where p_{wm} is a keypoint in $N(p)$ given by

$$p_{wm} = \arg\min_{p_r} \left| \sum_{i=1}^{r} w_i - 0.5 \right| \tag{7}$$

The wMd is an estimation to the disparity of p based on the disparities of its neighboring keypoints. Comparing with the mean value, the wMd is more robust to outliers with a large disparity deviation. As $\sum\limits_{p_r \in N(p)} w_r = 1$, the wMd is similar to the median value, but it favors the disparity of keypoints which are closer to keypoint p. As Fig. 1 shows, although the median of $N(p)$ is $d(p_6)$, but $d(p_4)$ resulting from wMd is a more accurate estimation of $d(p)$. Actually, the median

value can be obtained by setting w_r in Eq. (4) equal for all $p_i \in N(p)$.

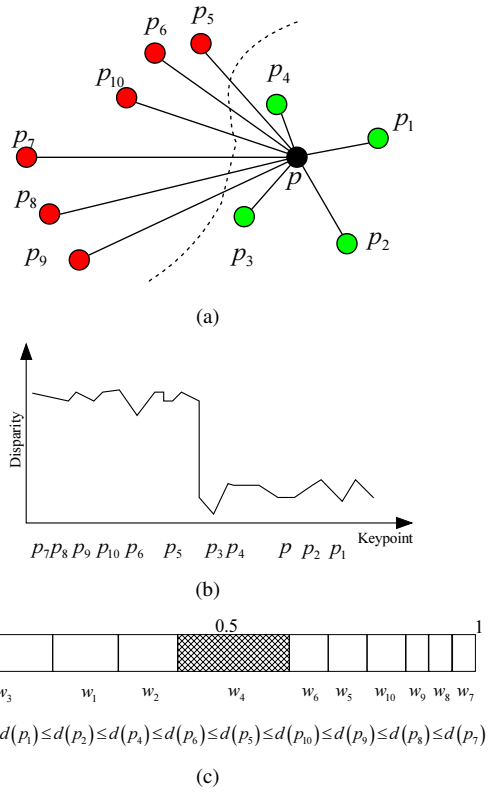

Fig. 1. Illustration of ADSF. (a) Keypoint p and the keypoints in $N(p)$, $p_{wm} = p_4$; dashline indicates an object boundary; green ones are the keypoints in $N_s(p)$, red ones are not included in $N_s(p)$; (b) The disparity of keypoints in (a); (c) The disparity relation and the weights of keypoints (the weight of p_{wm} is denoted by the shadow region).

$N(p)$ may contain some false matches or contain matches which are not on the same object. These matches should not be used when estimating the disparity of p. Considering the disparities of these matches are usually quite different from $d_{wm}(p)$, we define a subset on the matches whose disparities are close to $d_{wm}(p)$ by:

$$N_s(p) = \left(p_r \in N(p) \,\middle|\, |d(p_r) - d_{wm}(p)| < \beta\right) \tag{8}$$

where β is a threshold for filtering out the false matches and matches on the different objects (see Fig. 1(a)). The matches in $N_s(p)$ are expected to be the correct matches lying on the same object with keypoint p. If p is on a smooth object, the disparities of keypoints in $N(p)$ can be quite similar or even the same. In such a case, a small difference between the disparity of p and its estimation, $d_{wm}(p)$, will indicate a false correspondence. On the other hand, if the disparities of keypoints in $N(p)$ are different from each other, disparity of p may have a large difference from $d_{wm}(p)$. Thus, we decide whether the match of p is correct or not by:

$$|d(p) - d_{wm}(p)| < \gamma \cdot std(N_s(p)) \tag{9}$$

where $std\big(N_s(p)\big)$ is the standard deviation of the disparities calculated over the set $N_s(p)$; γ is the weight on $std\big(N_s(p)\big)$.

The match of p will be regarded as a correct match if Eq. (9) is satisfied, otherwise a false match. Parameters, α, β, and γ, should be set according to the distribution of keypoints and their disparities in the image, the estimation to these is given in Section II-D.

C. Disparity Estimation

Given the epipolar geometry between two views, the depth of a keypoint can be obtained from its coordinate and the coordinate of its correspondence in the other image. This relation is much simpler in the rectified image pair where the corresponding epipolar lines are arranged on the same horizonal scanline. In this case, the vertical disparity is zero, and the depth is only related to the disparity in the horizonal direction. Thus, 3D smoothness in the neighborhood of the sense is encoded by the disparity smoothness in the neighborhood of the rectified images.

The rectification is carried out by projecting the points in two images using two homographies respectively. The rectified coordinates of the matching pair (p, q) are given by

$$\begin{cases} p_r = H_1 p \\ q_r = H_2 q \end{cases} \tag{10}$$

where H_1 and H_2 are the two homographies which can be obtained from the method described in [21]. p_r and q_r are two rectified coordinates in the homogeneous coordinate system. Note that the vertical disparity may not be exactly zero for the rectified coordinates, since the F obtained in Section II-A may not be the perfect fundamental matrix, and the location error exists in the matching pair. As we employ the epiploar constraint in Section II-A to find candidate matches, the vertical disparity between two matching points is small. Thus, the disparity of a keypoint p is defined only by the horizontal disparity between its rectified coordinate and that of its correspondence:

$$d(p) = q_r(x) - p_r(x) \tag{11}$$

where $p_r(x)$ and $q_r(x)$ are the horizontal coordinates in inhomogeneous coordinate system of p_r and q_r respectively.

D. Adaptive Parameter Estimation

In this section, we will discuss how to estimate the parameters mentioned above: α, β, and γ. The disparity jump is defined as the difference of the disparity between a point p and its neighboring keypoints in $N(p)$. The disparity jump may be different from image to image. These parameters should be robust to the density of the keypoints in the image and the difference of disparity jump. For example, if the image is rescaled by 2 and we want to keep the weight in Eq. (4) fixed, the parameter α should be multiplied by 2 for the reason that the distance is doubled. If the image contains large disparity jumps, we will expect the parameters β and γ to be large. Similarly, small β and γ are preferred for the image where the disparity jump is small.

The parameter α in Eq. (4) is set to the mean of the distance between two neighboring keypoints. To estimate the parameters β and γ, we firstly create a disparity jump histogram over

all the disparity jumps between two neighboring keypoints in the image. Fig. 2 shows a disparity jump histogram, with each bin representing a value of an integer jump. As a disparity jump is a float number, the bilinear interpolation is used to put the counting of an entry with the jump value, j, into the two nearest integer disparity jump $j_+(j_+ > j)$ and $j_-(j_- < j)$. The counting for two nearest bins are given by $1-\Delta j$, where Δj is the absolute difference between j and j_+ (or j_-).

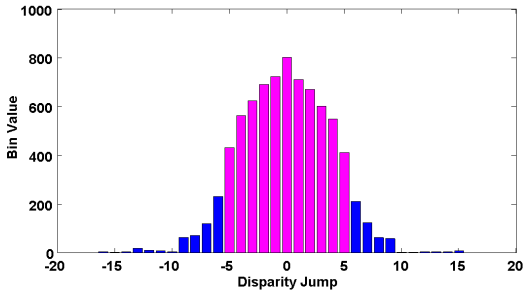

Fig. 2. An illustration of disparity jump histogram (pink bins represent the jumps within the range of $[-\beta, \beta]$, while blue ones are outside of this range).

The disparity jump of correct matches on the same object is usually small. Therefore those with a disparity smaller than β are considered to be the disparity jumps between correct matches on the same object. We predefined a confidence ratio, (C_r), which controls the ratio between the number of disparity jump within $[-\beta, \beta]$ against the number of all disparity jumps. For a given value of C_r (ranges from 0 to 1), we estimate the parameter β by

$$\begin{aligned} \beta &= \arg\min_{\beta_j} \left(\sum_{j=-\beta_j}^{\beta_j} h(j) \right) \\ \text{s.t.} \quad & \sum_{j=-\beta_j}^{\beta_j} h(j) \geq \sum_{j=-\infty}^{\infty} h(j) \cdot C_r \end{aligned} \tag{12}$$

where $h(j)$ is the value of the bin at jump j. The parameter γ is given by $\gamma = \beta / std_{|\beta|}$, where $std_{|\beta|}$ is the standard deviation of all disparity jumps within the range of $[-\beta, \beta]$ (see Fig. 2).

III. Finding Correspondences according to Distribution Density

In this step, we will find more correspondences especially in the region where the number of correspondence is low. We denote the set of the correspondences which are considered to be correct in ADSF by S_-. Let P_- and Q_- be two sets of keypoints in the source and reference images respectively corresponding with S_-. Thus, we will find the correspondences among the keypoints in $\overline{P}_-$ and $\overline{Q}_-$ which are the complements of P_- and Q_-.

For a given keypoint, p' ($p' \in \overline{P}_-$), the epipolar constraint and smoothness constraint limit the search range of its matching point in the reference image. According to the epipolar constraint, the position of q' and the position of its matching point p' should meet Eq. (2). Let $d_N(p')$ be the disparity of K-nearest neighboring keypoint ($K = 10$) of p' in P_-. According to the disparity smoothness constraint, the disparity jump should be smaller than β. Thus, the possible disparity range is given by $[\min(d_N(p')) - \beta, \max(d_N(p')) + \beta]$, where β is the same as in Eq. (12). These two requirements define the region of possible matching point in the reference image (see Fig. 3). As there is probably no keypoint meeting the two requirements, p' may have no matching points. Denote the best matching keypoint of p' among all possible matching points by q', and let (p', q') be a possible correspondence. If the feature distance between p' and q' is lower than a threshold $\tau(p', q')$, the possible correspondence will be regarded as correct. Following the uniqueness constraint, if more than one keypoint in an image has the same best matching keypoint in the other image, then only the one with the shortest feature distance will be counted. To make correspondences distributed as

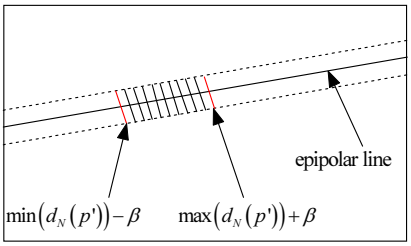

Fig. 3. An illustration of a region of possible matching point. Dash lines are the boundaries defined by the epipolar constraint; Red line are the boundaries defined by the smoothness constraint.

evenly as possible in the image, a higher threshold, $\tau(p', q')$, is preferred where fewer correspondences exist, so that more new correspondences can be found. For a correspondence (p', q'), the number of the correspondences in S_- within an $L \times L$ region around p' and q' respectively are denoted by $num(p')$ and $num(q')$. L is given by $\sqrt{\frac{Height \cdot Width}{Card(S_-)}}$, where $Height$ and $Width$ are the height and width of the image respectively; $Card(S_-)$ is the total number of the correspondences in S_-. The threshold $\tau(p', q')$ is then given by,

$$\tau(p', q') = \tau_r \left(1 - \frac{num(p') \cdot num(q')}{\max(num(p') \cdot num(q'))} \right) \tag{13}$$

where $\max(num(p') \cdot num(q'))$ is the maximum value among all possible correspondences detected; and τ_r is a predefined threshold. Any possible correspondence whose feature distance exceeds this threshold will be regarded as a false match. As we use the SIFT feature in our method, which is a normalized feature descriptor, τ_r ranges from 0 to 1. $\tau(p', q')$ is high where the correspondence density is low, otherwise it is low. It is a tradeoff between finding more correspondences and having a more even distribution.

The newly found correspondences may contain some false correspondences. So we perform ADSF on the set S_+ which is the union of the set of newly found correspondence and the set S_-. After ADSF, we find more correspondence once again as described above. Obviously, the set S_+ contains more accurate correspondence than S. Therefore, each time when we perform ADSF, C_r is increased by ΔC_r. Our method performs ADSF

and finding correspondence recursively, and stops when C_r reaches or exceeds 1. We found this recursive method performs much better than just performing once.

IV. Experimental Results

The proposed method in this paper is suitable for all applications where the images are captured from different view points of a static scene. In this section, we firstly show the robustness of our method against different parameters. Three aspects of the performance are tested in our experiments, i.e., the percentage of correct matches, the distribution of the correspondence, and the number of correspondence. Experimental results show that our algorithm outperforms the latest developed algorithm, the triangle constraint measurement (TCM) method [13].

A. Parameter Settings

To estimate the parameters, C_r, ΔC_r, and τ_r empirically, we compare our results with the ground truth under different parameters, using the Oxford data set [22]. For a match (p, q) obtained by our method, the two regions around p and q within 3 pixels are called corresponding regions. If at least one pair of matching pixel exists between two corresponding regions in the ground truth data, the match (p, q) will be regarded as an accurate match, otherwise a false match. Matches in the ground truth can be generated from the provided homography. This measurement is robust to the small location error of the keypoint at depth boundary. Fig. 4 shows the percentage of correct matches of our method on the "Graffiti" image, against the parameters C_r, and ΔC_r. Fig. 4(a) and Fig. 4(b) show the percentage of correct matches against C_r and ΔC_r by setting τ_r to constants 0.1 and 0.4 respectively. The percentage of correct matches is fairly constant with respect to different sets of C_r and ΔC_r.

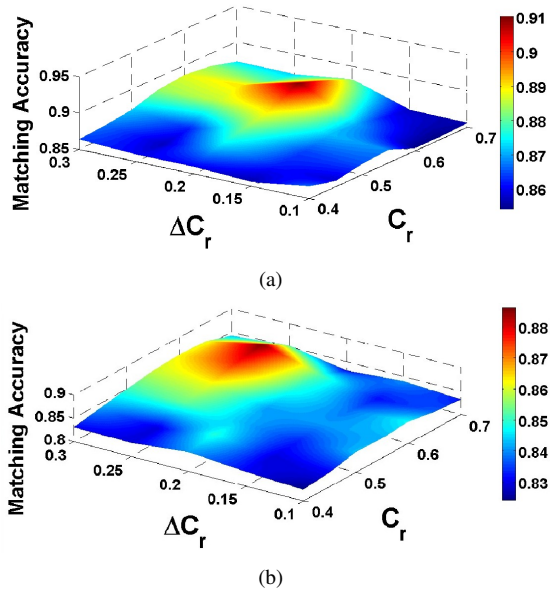

Fig. 4. Performance against the parameters C_r, and ΔC_r. (a) The performance by setting $\tau_r = 0.1$. (b) The performance by setting $\tau_r = 0.4$.

The parameter τ_r controls the number of total matches and the percentage of correct matches. A smaller τ_r results in a higher percentage of correct matches but fewer matches. On the other hand, a lower percentage of correct matches but more matches. Setting C_r and ΔC_r to constants, the performance of our method with respect to parameter τ_r is shown in Fig. 5. The τ_r is from 0.2 to 0.4, where most correct matches are found, and the percentage of correct matches is about 90 percent. Therefore, we choose $C_r = 0.6$, $\Delta C_r = 0.2$, $\tau_r = 0.3$ for the comparison between our method and the latest developed method, TCM [13].

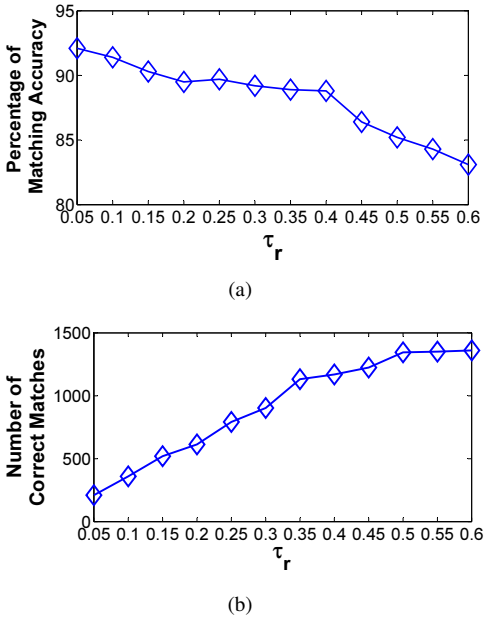

Fig. 5. Performance according to the parameters τ_r, by setting C_r, and ΔC_r to constants ($C_r = 0.6$, $\Delta C_r = 0.2$). (a) The percentage of correct matches. (b) The total number of correct matches.

B. Performance Evaluation

The evaluation of the performance of our method is carried out using the Middlebury data sets. Fig. 6 shows the source images of the data sets from Middleburry website [23]. We rotate the reference image with a random angle to make the test more general. The ground truth matches can be obtained from the provided disparity map. In the comparison, the best parameters ($\tau = 0.5$, $\lambda = 0.5$) in the TCM method are used as described in [13]. The performance evaluation is carried out on percentage of correct matches, number of correct matches, and the distribution of the matches which is measured using the standard deviation of the point density [16], which should be low for a better result. Table I gives the performance comparison between our method and TCM. Experiments show that the results from our method are much better than that of TCM.

Some more experiments are carried out using different types of out-door images. The results are also very good (see Fig. 7).

V. Conclusion

In this paper, we present a new method for finding feature correspondences between images. The proposed ADSF algo-

TABLE I
THE COMPARISON BETWEEN OUR METHOD AND TCM.

Image	Percentage of Correct Correspondences		Standard Deviation of Point Density		Total Number of Correct Correspondences	
	TCM	Our Method	TCM	Our Method	TCM	Our Method
teddy	89.2%	94.1%	2.11	1.36	124	321
cones	81.6%	96.8%	1.51	1.32	152	439
tsukuba	11.8%	96.5%	1.49	1.37	132	489
venus	98.5%	97.6%	1.57	1.35	65	385
art	76.4%	83.3%	1.95	1.35	165	359
cloth3	94.7%	98.8%	1.54	1.24	399	1148
laundry	75.0%	80.1%	2.44	1.24	284	637
dolls	89.5%	95.2%	2.74	1.29	275	579
aloe	90.6%	96.0%	1.50	1.27	509	920
books	91.1%	87.1%	1.65	1.37	124	440
bowling2	79.3%	86.4%	1.88	1.71	58	221
baby3	90.5%	92.4%	1.68	1.47	197	317

(a) teddy (b) cones (c) tsukuba

(d) venus (e) art (f) cloth3

(g) laundry (h) dolls (i) aloe

(j) books (k) bowling2 (l) baby3

Fig. 6. The images used to evaluate the matching performance.

rithm efficiently filters out false matches based on the disparity jumps of neighboring correspondences. More correct correspondences are then found based on the epiploar geometry and the distribution of the correspondences. A recursive method is used to combine the finding of more correct correspondences and the filtering out of false correspondences. In the experiments based on real images and their ground truth, our method performs very well on the aspects of percentage of correct matches, number of matches, and correspondence distribution, comparing with the state-of-the-art method. The experiments

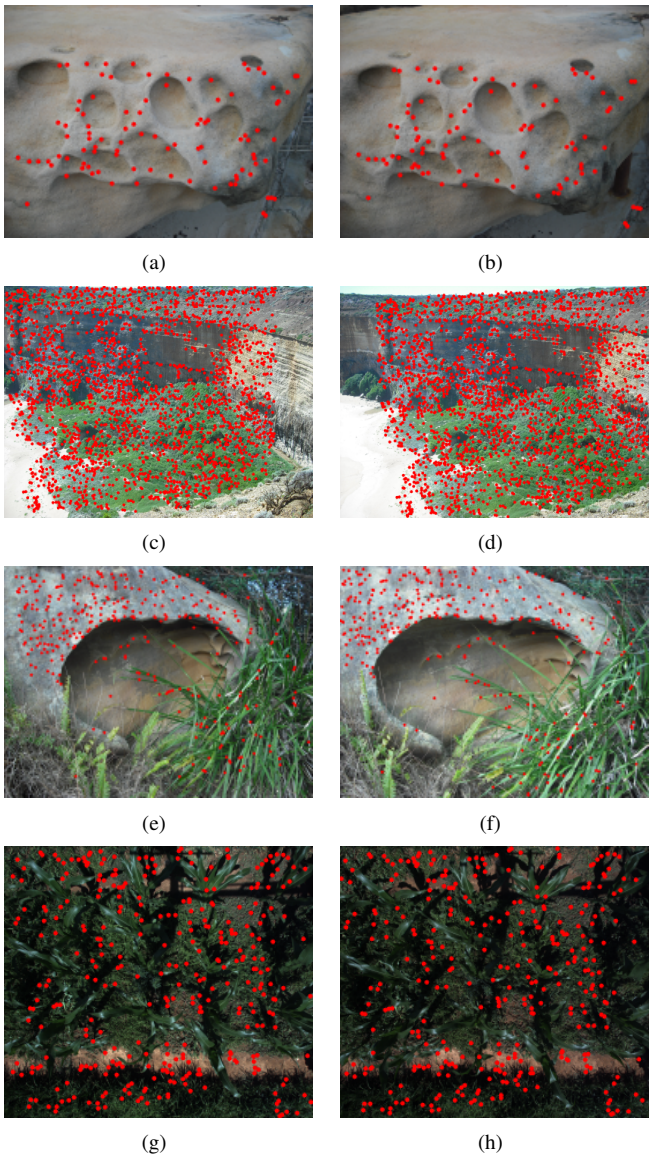

(a) (b)

(c) (d)

(e) (f)

(g) (h)

Fig. 7. The results of out-door real images.

with out-door real images, also prove the efficiency of our method.

ACKNOWLEDGMENTS

We thank Mohammad Hosseini for his comments on this paper. Tan was partially supported by the China Scholarship Council. Sun was partially supported by the CSIRO's Transformational Biology Capability Platform.

REFERENCES

[1] R. Hartley, "In defense of the eight-point algorithm," *PAMI*, vol. 19, no. 6, pp. 580–593, 1997.
[2] Z. Zhang, "Determining the epipolar geometry and its uncertainty: A review," *IJCV*, vol. 27, no. 2, pp. 161–195, 1998.
[3] E. Mouragnon, M. Lhuillier, M. Dhome, F. Dekeyser, and P. Sayd, "Real time localization and 3D reconstruction," in *CVPR*, vol. 1. IEEE, 2006, pp. 363–370.
[4] E. Tola, V. Lepetit, and P. Fua, "A fast local descriptor for dense matching," in *CVPR*. IEEE, 2008, pp. 1–8.
[5] Z. Zhang, "A flexible new technique for camera calibration," *PAMI*, vol. 22, no. 11, pp. 1330–1334, 2000.
[6] M. Cho, Y. Shin, and K. Lee, "Unsupervised detection and segmentation of identical objects," in *CVPR*. IEEE, 2010, pp. 1617–1624.
[7] S. Belongie, J. Malik, and J. Puzicha, "Shape matching and object recognition using shape contexts," *PAMI*, vol. 24, no. 4, pp. 509–522, 2002.
[8] D. Lowe, "Object recognition from local scale-invariant features," in *ICCV*, vol. 2. IEEE, 1999, pp. 1150–1157.
[9] K. Mikolajczyk and C. Schmid, "A performance evaluation of local descriptors," *PAMI*, vol. 27, no. 10, pp. 1615–1630, 2005.
[10] H. Bay, T. Tuytelaars, and L. Van Gool, "SURF: Speeded up robust features," *ECCV*, pp. 404–417, 2006.
[11] M. Leordeanu and M. Hebert, "A spectral technique for correspondence problems using pairwise constraints," in *ICCV*, vol. 2. IEEE, 2005, pp. 1482–1489.
[12] M. Brown and D. Lowe, "Recognising panoramas," in *ICCV*, vol. 2, 2003, pp. 1218–1225.
[13] X. Guo and X. Cao, "Good match exploration using triangle constraint," *Pattern Recognition Letters*, vol. 33, no. 7, pp. 872–881, 2012.
[14] J. Maciel and J. Costeira, "A global solution to sparse correspondence problems," *PAMI*, vol. 25, no. 2, pp. 187–199, 2003.
[15] Z. Zhang, R. Deriche, O. Faugeras, and Q. Luong, "A robust technique for matching two uncalibrated images through the recovery of the unknown epipolar geometry," *Artificial intelligence*, vol. 78, no. 1-2, pp. 87–119, 1995.
[16] J. Seo, H. Hong, C. Jho, and M. Choi, "Two quantitative measures of inlier distributions for precise fundamental matrix estimation," *Pattern Recognition Letters*, vol. 25, no. 6, pp. 733–741, 2004.
[17] H. Longuet-Higgins, "A computer algorithm for reconstructing a scene from two projections," *Nature*, vol. 293, pp. 133–135, 1981.
[18] P. Torr and D. Murray, "The development and comparison of robust methods for estimating the fundamental matrix," *IJCV*, vol. 24, no. 3, pp. 271–300, 1997.
[19] Y. Xu, D. Wang, T. Feng, and H. Shum, "Stereo computation using radial adaptive windows," in *ICPR*, vol. 3. IEEE, 2002, pp. 595–598.
[20] K. Yoon and I. Kweon, "Adaptive support-weight approach for correspondence search," *PAMI*, vol. 28, no. 4, pp. 650–656, 2006.
[21] R. Hartley, "Theory and practice of projective rectification," *IJCV*, vol. 35, no. 2, pp. 115–127, 1999.
[22] http://www.robots.ox.ac.uk/~vgg/.
[23] vision.middlebury.edu/stereo/.